POLISH MARITIME RESEARCH 2 (94) 2017 Vol. 24; pp. 27-39
10.1515/pomr-2017-0047

EFFECTS OF BOUNDARY LAYER CONTROL METHOD ON HYDRODYNAMIC CHARACTERISTICS AND TIP VORTEX CREATION OF A HYDROFOIL

Parviz Ghadimi[1)]
Araz Tanha[1)]
Navid Nemati Kourabbasloo[2)]
Sasan Tavakoli[1)]
[1)] Amirkabir University of Technology
[2)] Sharif University of Technology

ABSTRACT

There is currently a significant focus on using boundary layer control (BLC) approach for controlling the flow around bodies, especially the foil sections. In marine engineering this is done with the hope of increasing the lift – to – drag ratio and efficiency of the hydrofoils. In this paper, effects of the method on hydrodynamic characteristics and tip vortex formation of a hydrofoil are studied. Steady water injection at the tip of the hydrofoil is simulated in different conditions by using ANSYS-CFX commercial software. Validity of the proposed simulations is verified by comparing the obtained results against available experimental data. Effects of the injection on the lift, drag, and lift – to – drag ratio are studied and the ranges within which the injection has the most positive or negative effects, are determined. Furthermore, flow pattern and pressure variation are studied upon the water injection to determine the most positive and negative case and to ascertain the main reasons triggering these phenomena.

Keywords: steady water injection, boundary layer control, hydrofoil, NACA 0015, tip vortex

INTRODUCTION

In the previous studies related to the characteristics of aerofoils and hydrofoils, researchers have highlighted different three-dimensional phenomena affecting aerofoil efficiency. These effects can be the result of some of the aerofoil characteristics or corresponding phenomena such as aspect ratio [3] and tip-vortex [4-6]. Both aspect ratio and tip-vortex may result in a lower lift- to- drag ratio and reduce the efficiency of an aerofoil. In this regard, numerous attempts have been made to reduce the resulting negative effects and increase the efficiency of an aerofoil. However, it has always been attempted to reduce the negative effects and increase the efficiency of a foil. One of the best methods for increasing the efficiency is controlling the flow around the body. Englar [7,8] presented one of the earliest research in this field. Its main aim was to control the circulation around airfoils in order to reach a higher lift – to -drag ratio. However, no result regarding the behaviour of tip vortices during fluid injection was presented. Wood and Nielsen [9] conducted a literature review regarding this issue. Wood and Robert [10] also presented a blowing method for controlling the lift of Delta Wings. Wood *et al.* [11] proposed another control method for increasing the efficiency of aerofoils. In another work, Modi *et al.* [12] offerred a method for reducing the drag of bluff bodies by using boundary layer method. They proposed a control method for the lift of aerofoils by using separation control. Their results confirmed that the proposed method was suitable for drag reduction; however, they did not provide any details regarding the flow regime, when they performed the controlling method. Moreover, by using boundary layer separation control, Johari and McManus [13] discussed the effect of controlling methods on efficiency of the aerofoils. By using a pulsed jet controlling the separation on the boundary layer of the flow, McManus and Magili [14] also presented a different approach for increasing the lift of aerofoils. Furthermore, Zha and Paxton [15] proposed a method called

co-flow jet in order to enhance the efficiency of aerofoils. Zha *et al.* [16] also employed this method to investigate its viability when the aerofoils are in high performance.

Gilarranz *et al.* [17] initiated a method for controlling flow around bodies, which was later experimentally applied to NACA 0015 aerofoil [18]. You and Moin [19] also performed a Large-Eddy Simulation (LES) in order to control the flow around a NACA 0015 aerofoil and further verified their simulation by comparing their results against experimental measurements by Gilarranz *et al.* [18]. Their numerical approach and controlling method were based on a harmonic injection. Agarwal et al. [20] conducted an experimental investigation on the pulsed air blowing separation control for a NACA 0015 aerofoil. They observed the effects of injection frequency on the flow. Similarly, Mack *et al.* [21] presented experimental results of flow control method for aerofoils. Later, Gompetz and Brunes [22] made an attempt to control the flow around aerofoil section of the wind turbines.

In recent years, Packard *et al.* [23] conducted experiments based on steadily blown injection and found the best conditions for controlling the flow over NACA 643-618 aerofoil. Also, Gardner *et al.* [24] experimentally measured the variation of stall angle caused by high-pressure blowing. Moreover, Zhang and Samtaney [25] employed Direct Numerical Simulation (DNS) to investigate the effects of frequency on the boundary layer separation control. Furthermore, Meng *et al.* [26] studied the plasma-laminar separation bubble control over aerofoils. Also, Hipp *et al.* [27] performed a numerical simulation in order to investigate the control of the flow in leading-edge of an aerofoil. Finally, Bernardini *et al.* [28] performed a numerical research in order to obtain the oscillation of flow characteristics due to flow control over an aerofoil. However, all of the presented methods have not provided sufficient information regarding the tip vortices and the behaviour of the regime during the flow injection. This is why the tip vortices are the main reason triggering three dimensional negative effects.

In this paper, NACA 0015 hydrofoil is selected to investigate the steady water injection effects on the flow in vicinity of the hydrofoil tip. The hydrofoil is considered in two different conditions : with and without tapper ratio. The ANSYS-CFX software is utilized and k-ω SST turbulence model is employed in order to obtain the flow over the hydrofoil. Lift, drag, and efficiency coefficients are determined during water injection at the tip of the hydrofoil. The velocity and pressure distribution over the hydrofoil are also studied, which can be instrumental in further understanding of the effects of steady injection of water at the tip of a hydrofoil. Also, the tip vortices flow before and during the injection is determined.

MATHEMATICAL FORMULATION

PROBLEM DEFINITION

In the current paper, it is assumed that a submerged hydrofoil is exposed to a flow with the speed U directed against the angle α, as shown in Fig. 1. In this condition, the Reynolds number is defined as

$$\mathrm{Re} = \frac{Uc_{\mathrm{R}}}{\upsilon} \tag{1}$$

where c_{R} is the chord length of the foil at its root section and ν is considered to be the fluid kinematic viscosity equal to 0.894×10^{-6} m^2/s. For the current research, c_{R} is considered to be 1 m. Also, it is assumed that the hydrofoil has a taper ratio identified by

$$\mathrm{TR} = \frac{c_{\mathrm{T}}}{c_{\mathrm{R}}} \tag{2}$$

in which subscripts T and R refer to hydrofoil tip and root, respectively. It is also supposed that the incompressible flow with the speed V is injected at the tip of the foil with the angle θ with respect to the horizontal line. It should be noted that the flow is only injected in the zy-plane. The ratio of the flow speed and the injection speed is defined as "U/V speed ratio". The coefficient (C_L) of the lift force L acting on the hydrofoil is computed as follows:

$$C_{\mathrm{L}} = \frac{L}{\frac{1}{2}\rho U^2 A_F} \tag{3}$$

and the coefficient (C_D) of the drag force D is determined by using the formula

$$C_D = \frac{D}{\frac{1}{2}\rho U^2 A_F} \tag{4}$$

where : A_F is the total wing area, i.e. that which contains the areas of the upper and lower surfaces.

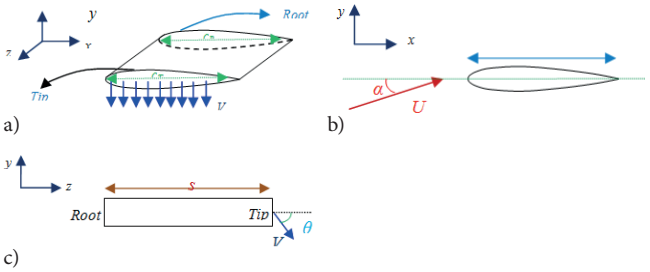

Fig. 1. Illustration of the considered problem: (a) three-dimensional view, (b) side view, (c) front view.

GOVERNING EQUATIONS

It is assumed that the fluid is incompressible and viscous. Therefore, the governing continuity equation can be written as

$$\frac{\partial \rho}{\partial t}+\frac{\partial}{\partial x_i}(\rho u_i)=0 \qquad i=1,2,3 \tag{5}$$

Also, the governing momentum equation is

$$\frac{\partial}{\partial t}(\rho \overline{u_i})+\frac{\partial}{\partial x_j}(\rho\,\overline{u_i u_j})=-\frac{\partial \overline{p}}{\partial x_i}+\frac{\partial}{\partial x_j}(\overline{\tau}_{ij}-\rho\,\overline{u_i' u_j'}) \tag{6}$$

where

$$\overline{\tau}_{ij}=\mu\left(\frac{\partial \overline{u}_i}{\partial x_j}+\frac{\partial \overline{u}_j}{\partial x_i}\right) \tag{7}$$

In the current paper, these equations are solved by using the commercial software Ansys-CFX previously employed also by several researchers [29-32]. The *k-ω* SST turbulence model adopts the same approach. The transport equation of *k-ω* SST turbulence model may be written as follows :

$$\frac{\partial}{\partial t}(\rho k)+\frac{\partial}{\partial x_j}(\rho u_j k)=\tilde{P}_k-\beta^*\rho k\omega+\frac{\partial}{\partial x_j}\left[(\mu+\sigma_k\mu_t)\frac{\partial k}{\partial x_j}\right] \tag{8}$$

$$\frac{\partial}{\partial t}(\rho\omega)+\frac{\partial}{\partial x_j}(\rho u_j \omega)=\alpha\rho S^2-\beta^*\rho\omega^2+\frac{\partial}{\partial x_j}\left[(\mu+\sigma_\omega\mu_t)\frac{\partial \omega}{\partial x_j}\right]+2(1-F_1) \tag{9}$$

The details of the parameters and their derivation can be found in Menter's report [33]. In the following subsections, the modelling method is described.

NUMERICAL MESHING

Geometry related to the numerical modelling of the presented problem is displayed in Fig. 2. As depicted in Fig. 2, there are six planes and one body. No-slip boundary condition is prescribed at the hydrofoil wall and the hydrofoil root is located on the efgh-plane. Three of the planes including abfe-plane, bcgf-plane and dcgh-plane, represent the domain inlet. Also, front and back boundaries are considered to have a symmetry boundary condition. Finally, the adhg-plane represents the domain outlet plane. Information related to the boundaries is shown in Tab. 1.

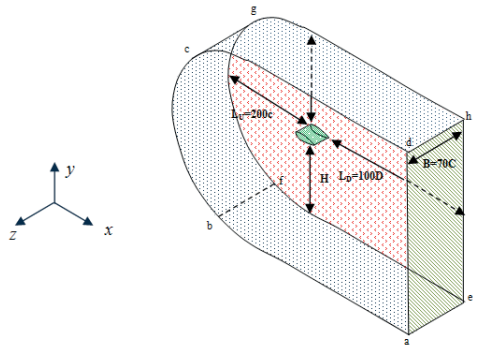

Fig. 2. Illustration of the problem domain

Tab. 1 Boundary conditions of the considered problem

Boundary	Condition
Hydrofoil	Wall(no slip)
abfe-bcgf-dcgh	Inlet
abcd-efgh (Front and Back)	Symmetry
Adhe	Outlet

NUMERICAL MODELLING

In the present simulations, a structured mesh is generated. Each cell has a hexahedron shape which can enhance the simulation quality of the tip vortices at the tip of the hydrofoil. Hence, such approach will yield more accurate results for this specific problem. Since the variation of physical parameters of the fluid flow in the neighbourhood of the hydrofoil is dramatic, the generated mesh in vicinity of the hydrofoil should be highly compact in comparison with the far field. Accordingly, to achieve more precise results at the tip of the hydrofoil at which tip vortices exist, mesh is generated with a higher density at the foregoing location. The schematic diagram of the generated mesh is depicted in Fig. 3. The above-mentioned solver of the Ansys-CFX code uses the FVM (Finite- Volume- based Finite Element) discretization technique for numerical solution of the problem [34].

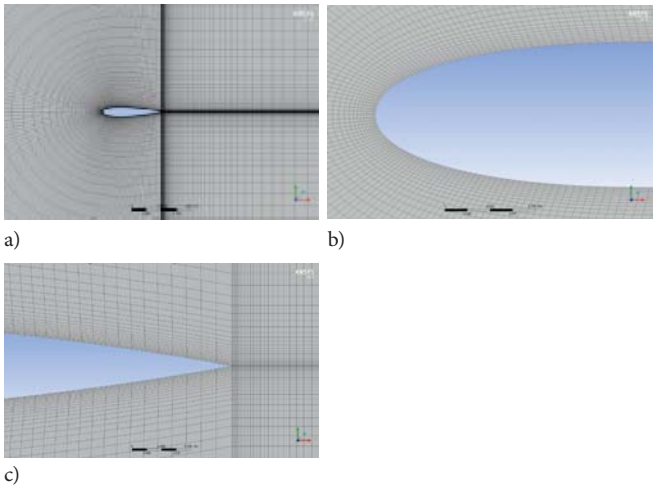

a) b)

c)

Fig. 3. Schematic diagram of the generated mesh: a) longitudinal section, b) close-to view at leading edge of wing tip , c) close-up view at trailing edge of wing tip

DOMAIN AND GRID-REFINEMENT STUDY

In this section, a study is carried out on the sensitivity of the results on grid density. In order to find the most efficient numerical mesh formation, the study is performed based on the lift coefficient results. To start with, a coarse mesh is generated with 1 200 000 cells. Subsequently, the lift coefficient for a hydrofoil with TR=1 at Re = 1 000 000, $\alpha = 6.5$ and $\theta = 45$ is computed. Afterward, a medium mesh and a fine mesh are generated with 2 500 000 and 3 400 000 cells, respectively. Again, lift coefficient for both fine and medium mesh are computed. A clustered column is displayed for this study in Fig. 4. As observed in this figure, the difference between lift coefficients for medium and fine mesh is very small. Therefore, the numerical solution process performed for the medium mesh may result in time saving. Accordingly, the medium mesh is adopted.

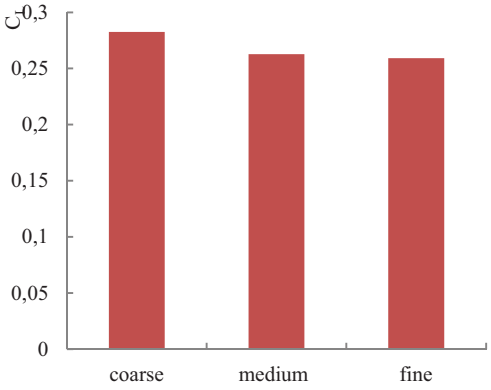

Fig. 4. Lift coefficient versus kind of mesh

VALIDATION

The present simulation is verified by comparing the computed pressure against the experimental results of Gilarranz *et al* [18]. Flow over a NACA 0015 foil was controlled by them at the frequency of 130 Hz and α=27.2. In the conducted simulations, flow was injected with jet momentum coefficient of $C\mu$=0.0254 at the tip of foil. The parameter $C\mu$ is defined as follows [35]:

$$C_\mu = \rho h u_N^2 / (\rho x_{REF} U_{REF}^2) \quad (10)$$

In which h is the width of neck, u_N is the amplitude of neck, x_{REF} is the chord length and U_{REF} is the free stream velocity. This parameter indicates the ratio of the neck momentum to free- stream momentum.

$C\mu$ may be also obtained by using the RMS value of the exit slot velocity or even the average value of the velocity at the jet exit slot. The comparison between the computed pressure and experimental results are displayed in Fig. 5. As evident in this figure, the numerical results and experimental data are in good agreement. Experimental data corresponding to fluid injection are very limited for further verification. However, the accurate pressure distribution presented for α = 27.2 can be considered a reliable criterion for capturing the overall trends for different simulations.

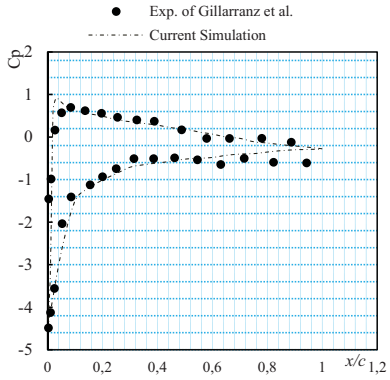

Fig. 5. Comparison of computed and measured data [18] for NACA 0015 foil at f=137 Hz, Cμ=0.0254 and α=27.2.

RESULTS

The problem analysed in the current study is related to a NACA0015 foil with the aspect ratio of 3 and TR of 1 and 0.7. The Reynolds number is assumed to be 1 000 000. Two angles of attack : $\alpha = 6.5$ and 17 degrees are taken into account. The injection velocity is 1 [m/s] and the injection angle (θ) varies from -20 degrees to 70 degrees. For each injection angle, a numerical simulation is conducted. The results are organized in three different sections. In the first section, lift, drag, and efficiency coefficients are presented. In the second part, flow pattern and velocity distribution during the injection are studied. Ultimately, pressure distribution over NACA 0015 hydrofoil is presented during the steady injection of water.

Tab. 2. Characteristics of the considered cases

	Case 1	**Case 2**
Span	3	3
TR	1	0.7
Chord length at tip	1	0.7
Chord length at root	1	1
Aspect ratio	3	3
Re	1e6	1e6
α	6.5-17	6.5-17
θ	-20 ~ +70	-20 ~ +70
U/V	0.894	0.894

HYDRODYNAMIC CHARACTERISTICS AND EFFICIENCY RATIO

In this section, the effects of fluid injection on the hydrodynamic coefficients are studied, first. The lift force coefficient (C_L) is computed for the hydrofoil at α=6.5 and

17 degrees and various injection angles for two taper ratios. For computing the C_L for the foregoing cases, the lift force is considered to be associated only with the pressure integration on the hydrofoil surface and the fluid injection momentum is not taken into account. In Fig.6 and 7, the effects of injection angle are illustrated. Regarding the injected fluid direction, no momentum component exists in the drag force direction. Both the injected flow location and velocity profile affect the lift variation. When the injection angle increases from -20 to 0 [deg], C_L increases. On the other hand, it is demonstrated that an increase in the injection angle from 0 to 70 degree results in lift coefficient reduction. Therefore, it can be concluded that the interaction between the injected fluid and the tip vortices occurring on the hydrofoil tip varies the pressure field and consequently, the lift coefficient declines. It should be noted that, according to Fig.6, the increase in the lift is of the same order as the accuracy of the method. However, the method is reliable enough for finding the overall trend of the lift. In order to verify this statement, a finer grid should be selected which is computationally very expensive in case of this problem. The interaction between injected fluid and tip vortices effects on the pressure field are thoroughly discussed in subsection 2.4.

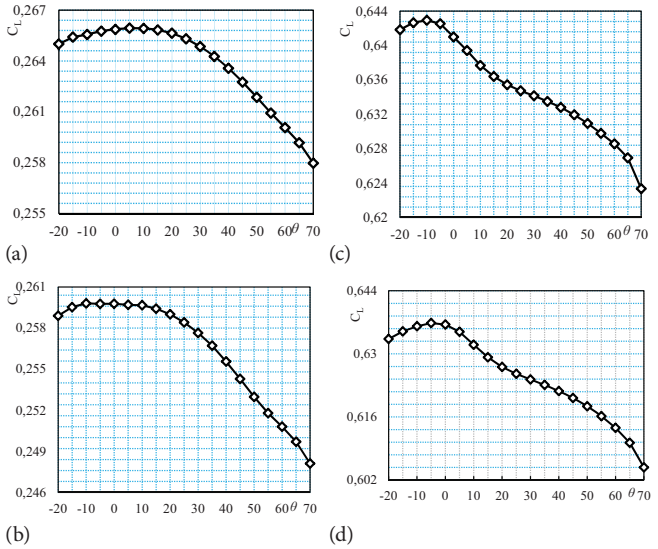

Fig. 6. Effect of injection angle on CL : (a) α=6.5 , TR= 0.7; (b) α=6.5 , TR= 1; (c) α=17 , TR= 0.7; (d) α=17 , TR= 1

In Fig. 7, variation of drag coefficient is plotted versus injection angle. As the injection angle increases from -20 to 70 degrees, the drag coefficient declines. The interaction between the tip vortices on the lower side , the upper side, and the injected fluid in vicinity of the hydrofoil tip results in the foregoing decrease in the lift coefficient. As a result of this interaction, the cross-flow is generated partially away from the hydrofoil tip; hence, the effect of the cross-flow on the hydrofoil grows weaker and consequently, the induced drag diminishes. It is also observed in Figs. 7(a) and 7(b) that an increase in the injection angle from 60 [deg] on, reverses the trend of the drag coefficient variation.

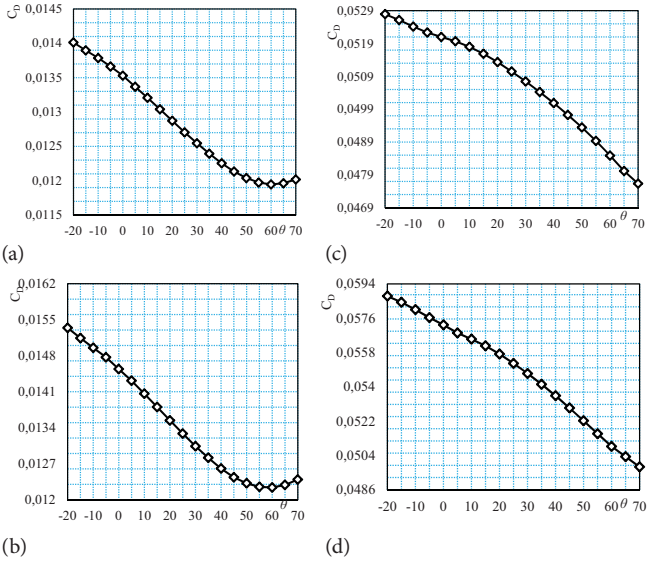

Fig. 7. Effect of injection angle on CD : (a) α=6.5 , TR= 0.7; (b) α=6.5 , TR = 1; (c) α=17 , TR= 0.7; (d) α=17 , TR= 1

The trend of efficiency versus the injection angle is shown in Fig. 8. In this work, efficiency is defined as

$$\eta = \frac{C_L}{C_D} \tag{10}$$

In all run cases, it is exhibited that as the injection angle increases, the efficiency increases. As shown in Fig. 6 and 7, when the injection angle increases, lift coefficient rises and drag coefficient declines. With regard to the efficiency definition, the drag coefficient decline is more significant than the augmentation of the lift coefficient; consequently, efficiency rises. In contrast, from the angle of 60 [deg] on, due to the drag coefficient increase (Figs. 6 (a) and 6 (b)), the efficiency lowers (Fig. 8 (a) and 8 (b)).

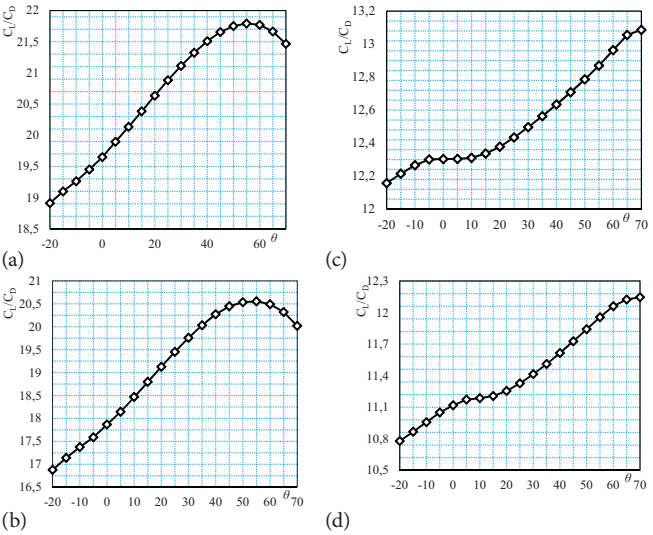

Fig. 8. Effect of injection angle on CL/CD : (a) α=6.5 , TR= 0.7; (b) α=6.5 , TR= 1; (c) α=17 , TR= 0.7; (d) α=17 , TR= 1

In order to investigate the performance of the proposed method, the results should be compared against the run cases without injection. To indicate the fluid injection performance, a parameter has been defined. This parameter - called Efficiency Variation Percentage- is defined as follows:

$$V\% = \frac{\frac{C_L}{C_D} - \frac{C_L^*}{C_D^*}}{\frac{C_L^*}{C_D^*}} \times 100 \tag{11}$$

where superscript * refers to the case without injection. Efficiency variation percentage for the run cases with injection and without injection is displayed in Fig. 9. According to Fig. 9(a), 9(b), and 9(d) at the angle of attack ranging from -20 to 20, -20 to 25, and -20 to 45 degrees, respectively, the flow injection has a negative effect on the hydrofoil performance. It is observed that maximum effectiveness of the fluid injection occurs at fluid injection angles of 55 and 70 degrees. It can be inferred from Fig. 9(c) that at all fluid injection angles, the performance is negative. Therefore, regarding the injection location, velocity profile and its value, this method is not suitable for the case (c).

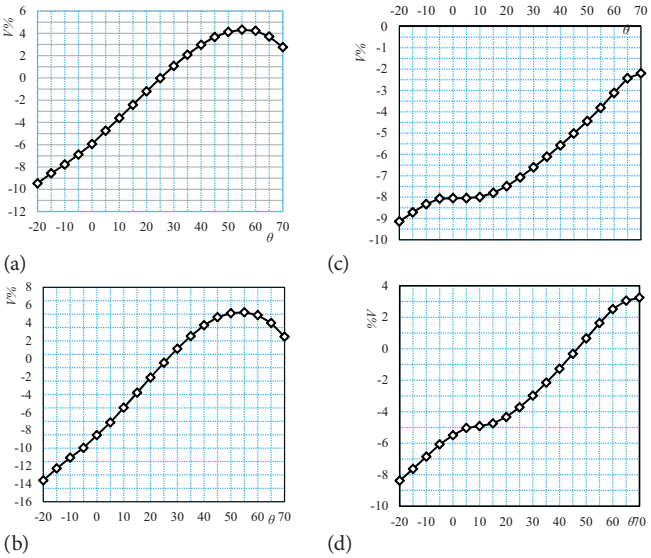

Fig. 9. Effect of injection angle on V% : (a) α=6.5 , TR= 0.7; (b) α=6.5 , TR= 1; (c) α=17 , TR= 0.7; (d) α=17 , TR= 1

FLOW PATTERN

Fig. 10 is presented to indicate the sections and lines utilized for the analysis of flow pattern and pressure coefficient distribution.

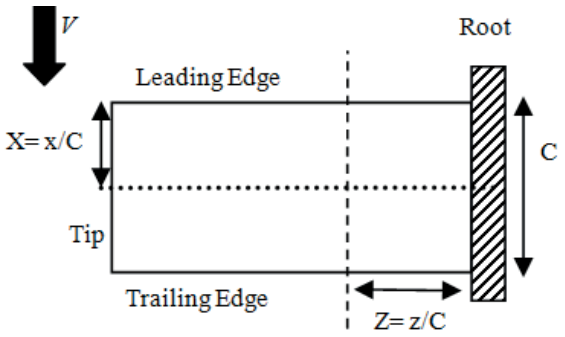

Fig. 10. Schematic profile of cross -section and transverse section

X is a non-dimensional parameter which is defined by

$$X = \frac{x}{C} \tag{12}$$

$$Z = \frac{z}{C} \tag{13}$$

where z is the distance from the hydrofoil root to a cross-section. In the present and following subsections, the effect of the injected fluid on the flow pattern and pressure coefficient distribution around the hydrofoil is investigated. To illustrate these effects, the results of two simulations are presented (case 1 and case 2) as shown in Tab. 3.

Tab. 3. Flow pattern and pressure coefficient distribution for the investigated cases.

	Case 1	Case 2	Case 3
A	6.5	6.5	6.5
Θ	-20	+55	Without Injection
TR	1	1	1
C_L	0.2589	0.25179	0.23174
C_D	0.015341	0.01225	0.011862
Re	1e6	1e6	1e6
U/V	0.894	0.894	0

As shown in Fig. 9, the positive effect of the fluid injection on efficiency in case 1, compared to the case without fluid injection, is the least. In case 2, the most positive impact on the efficiency, compared to the run case without fluid injection, is observed. In this section, the effect of the fluid injection on the flow pattern near the upper surface of the hydrofoil is investigated. Accordingly, the distribution of the velocity component w along the line perpendicular to the hydrofoil chord line is analysed. According to Fig. 10 and 11, the perpendicular lines are defined by X and Z. Values of the coordinates are given in Tab. 4.

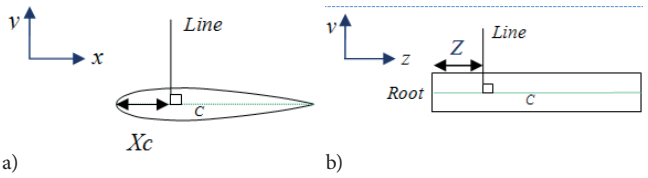

Fig. 11. The designated perpendicular lines whose coordinates are indicated in Tab. 4

Tab.4. Perpendicular line coordinates for the flow pattern investigation

	X	Z
Line 1	0.5	0.5
Line 2	0.5	1.4
Line 3	0.5	2
Line 4	0.5	2.7
Line 5	0.5	2.8
Line 6	0.5	2.9
Line 7	0.2	2.9
Line 8	0.4	2.9
Line 9	0.6	2.9
Line 10	0.8	2.9

As shown in Fig. 12(a), the variation of the velocity component *w* is insignificant in cases 1, 2 and 3, in comparison with each other. Regarding the location of line 1 (adjacent to the hydrofoil root), the tip vortices effects on the vicinity of this region is minimal. Similarly, as shown in Fig. 12(a) and 12 (b), the order of this variation is 0.001. However, in comparison with the previous figures, this variation has substantially increased. This trend seems logical, since line 1 in comparison with line 2, is closer to the hydrofoil tip; consequently, the effects of the interaction of the tip vortices and injected fluid on the velocity component on line 2 is a bit more significant. As it is observed, the resulting velocity component *w* near the upper surface of the hydrofoil in cases 1 and 2 is lesser than in case 3 due to the above mentioned effects. Moreover, according to Fig. 12(c) and 12(d), it can be claimed that the velocity component w, close enough to the surface, in case 1 is lesser than in case 2. However, far from the surface, *w* -component increases. Indeed, vortices are washed away from the upper surface of hydrofoil due to injection angle in case 1. Therefore, it can be concluded that the effects of fluid injection are more significant in vicinity of the upper surface of the hydrofoil in case 1, in comparison with the case 2. In Fig. 12(d), compared to Fig. 12(a), (b) and (c), it can be seen that the absolute value of the velocity component *w* has increased, since this line is located adjacent to the hydrofoil tip, and the tip vortices effects on this area are very substantial. In these figures, the comparison between the cases 1 and 2 clearly illustrates that in region close to the surface, the velocity component *w* in the case 1 is smaller than in the case 2 ($0 < y < 0.3$). However, at farther distance from the surface, the velocity component *w* is larger in the case 1 than in the case 2. Generally, it can be observed that in the vicinity of the hydrofoil tip, the positive effects of injection (reduction of the velocity component *w*) on the upper surface of the hydrofoil in the case 1 are greater than in the cases 2 and 3.

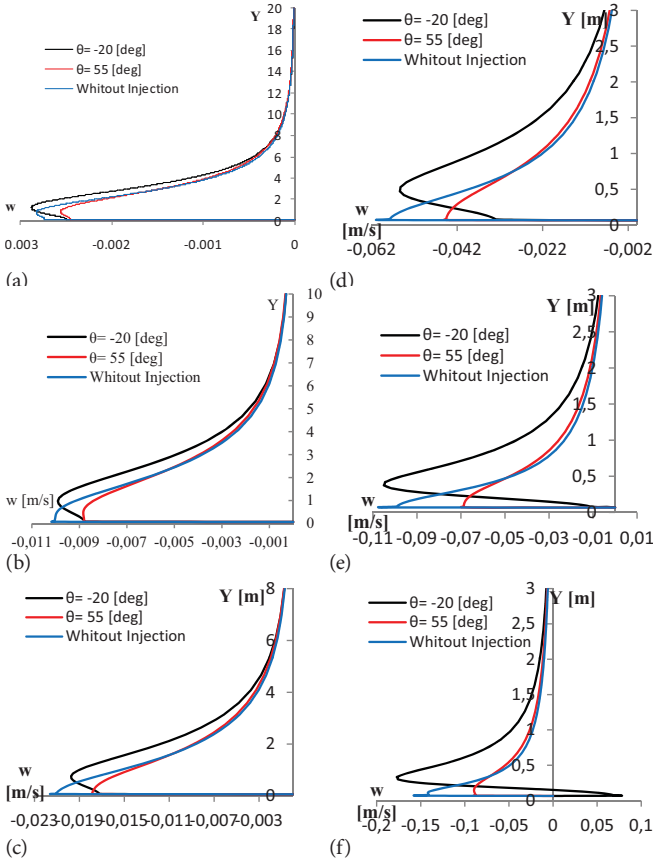

Fig. 12. Distribution of the velocity component w: (a) Z=0.5; (b) Z=1.4; (c) Z=2 ; (d) Z=2.6 ; (e) Z=2.8 ; (f) Z=2.9

The velocity distribution diagram has been plotted for the lines 6 to 10 in Fig. 13. As listed in the Tab. 4, these lines are located at the tip leading edge to the tip trailing edge of the hydrofoil. Generally, it can be observed that in the region close to the upper surface of the hydrofoil, the velocity component *w* for the case 1 from the lines 6 to 10 (Fig. 13(a) and 13(d)) is smaller than in the cases 2 and 3, and finally in the area close enough to the surface of the hydrofoil tip, this value changes to positive. This is well associated with the flow injection and the closeness to the hydrofoil surface, which in turn prevents the cross-flow from formation, and thus the velocity *w* becomes smaller, and consequently its sign changes into positive (Fig. 13 (d)). As shown in Fig. 6, it can be observed that the lift coefficient in the case 1 is greater than in the case 2, which is well associated with the reduction of the velocity component *w* in vicinity of the hydrofoil , that demonstrates the reduction of the cross-flow effect. According to Fig. 13, it can be seen that at the farther locations from the upper surface of the hydrofoil, the absolute value of the velocity component *w* for the case 1 is greater (more negative) than its value in the cases 2 and 3. Certainly, regarding the fluid

injection angle of -22 degrees, it can be concluded that vortices are formed at the farther distance from the hydrofoil upper surface in the case 1 comparing to the cases 2 and 3. In other words, they are washed away in the upward direction; hence, the negative effects of vortices on the velocity component *w* can be sensed at the farther distance. In all of the plots in the case 2, the velocity component w is smaller than its value in the case 3. This clearly shows that fluid injection prevents the cross-flow from formation in the vicinity of the hydrofoil. In this case, vortices are led toward the lower surface of the hydrofoil, and consequently smaller value of the velocity component *w* is obtained.

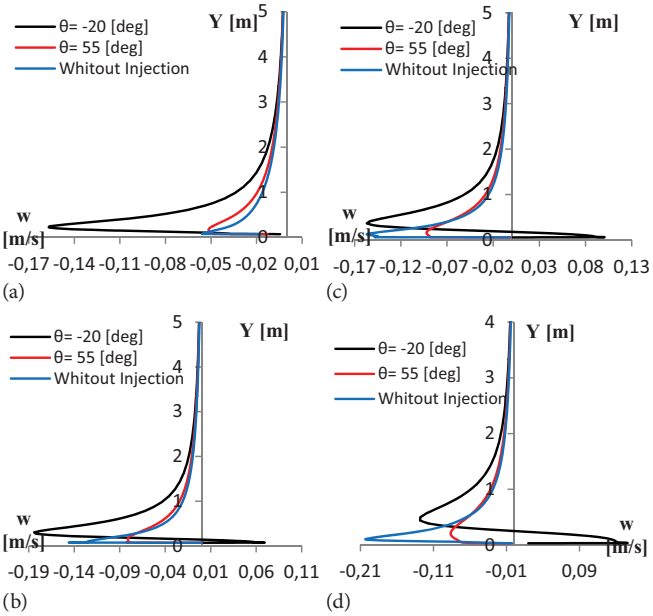

Fig. 13. Distribution of the velocity component w: a) X=0.2; (b) X=0.4; (c) X=0.6 ; (d) X=0.8

PRESSURE

In this section, the effects of the fluid injection on the pressure distribution over the surface of the hydrofoil are examined. Like in the section 4.2, the run cases 1 and 2 are selected and analyzed. Pressure distribution in the cross and transverse sections are examined. The cross and transverse sections are depicted in Fig. 10. *X* is a non-dimensional parameter, as shown in Fig. 10. Four sections are chosen for both cross and transverse orientations. The transverse sections $X = 0.2$, $X = 0.4$, $X = 0.6$ $X = 0.8$ and the cross sections $Z = 1$, $Z = 1.7$, $Z = 2.7$, $Z = 2.8$ and $Z = 2.9$ are considered. It should be noted that for the evaluation of effectiveness range, the effect of the interaction between the injected fluid and the cross-flow on pressure distribution is considered at the cross sections $Z = 1$ and $Z = 1.7$ for the cases 1 and 2, respectively. Firstly, in order to investigate the effects of the injected fluid on the pressure distribution, the graph of pressure coefficient distribution is drawn at the specified sections for the cases 1 and 3 , that is depicted in one plot in Fig. 14 and 15. Fig. 14(a) shows the distribution of the pressure coefficient *Cp* of the hydrofoil at the transverse section $X = 0.2$. This figure clearly illustrates the effects of the injected fluid on *Cp*-distribution in comparison with the run case without fluid injection. It is evident that the pressure difference between the upper and lower surface of the hydrofoil increases during the fluid injection, and consequently the lift force increases. Moreover, pressure variation in the run case without fluid injection is significant from $Z = 1.8$ to $Z = 3$. However, during the fluid injection, the variation begins farther from the root in comparison with the run case without fluid injection ($Z = 2.5$ to $Z = 3$) that well proves the effect of the fluid injection.

Fig.14 (b) displays the pressure coefficient distribution of the hydrofoil at the cross section $X = 0.4$. In comparison with the cross section $X = 0.2$, for the cases with fluid injection the pressure variation occurs at lower *Z* (i.e. $Z = 2$ to 3). The pressure variation in the run case without fluid injection occurs at $Z = 1.1$ to $Z = 3$. Evidently, the difference in pressure distribution for the upper and lower surface of the hydrofoil increases during the fluid injection, and as a result, the lift increases. Generally, these observations clearly demonstrate the effect of fluid injection. It is also seen that, at cross section $X = 0.4$, the lift coefficient distribution is less advanced than its distribution at the cross section $X = 0.2$.

Like in the cross sections $X = 0.2$ and $X = 0.4$, as it is shown in Fig. 14(c) and (d), in the run case with the fluid injection, the pressure difference between the lower and upper surfaces of the hydrofoil is higher than in the run case without fluid injection. The pressure difference on the upper and lower surfaces does not drop, as the injected fluid at the hydrofoil tip hinders cross-flow formation. During the fluid injection at the tip of the hydrofoil ($Z = 3$), velocity increases significantly; hence, comparing to the run case without fluid injection a steep reduction in *Cp*- coefficient value can be seen in all cases with fluid injection. In the considered case with fluid injection, pressure variation at the tip of the hydrofoil for all cross sections is smoother than in the case without fluid injection, and a comparably negligible jump is detected.

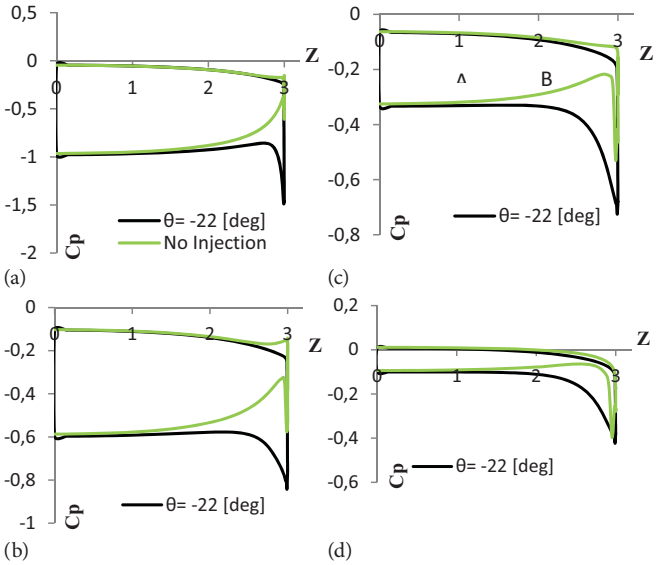

Fig. 14 Effect of injection angle on distribution of the pressure coefficient Cp in the case 1 : (a) X=0.2; (b) X=0.4; (c) X=0.6 ; (d) X=0.8

In Fig. 15, pressure coefficient distribution on the cross section is plotted. To study the effects of fluid injection on the hydrofoil, Fig. 15 (a) has been sketched. As it is shown in this figure, the injected fluid does not have a significant effect on the pressure coefficient distribution at $Z = 1.7$ in comparison with the run case without fluid injection. The effects of the injected fluid exist at $Z = 1.7$ to $Z = 3$. In the plots 15(b), (c), and (d), it is clearly demonstrated that during the fluid injection, the pressure coefficient difference between the upper and lower surfaces increases in comparison with the run case without fluid injection. In other words, fluid injection prevents the vortex formation (the velocity component w decreases) at the tip of the hydrofoil, and consequently hinders the pressure drop. This justifies in a different way the increase in lift in the run case with fluid injection in comparison with the run case without fluid injection.

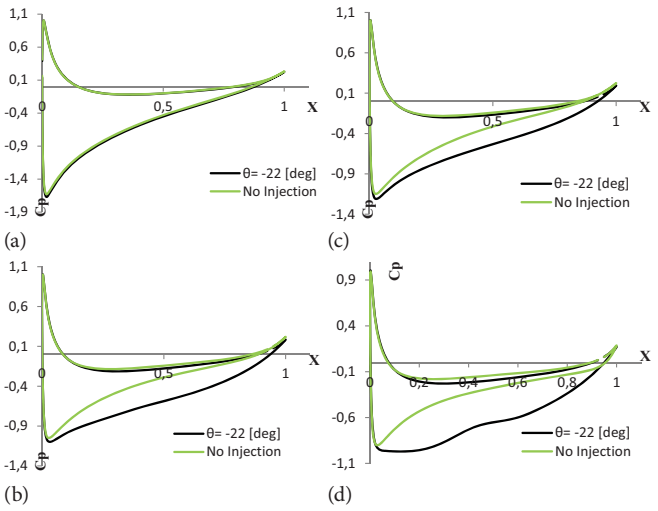

Fig. 15. Effect of the injection angle on distribution of the pressure coefficient Cp in the case 1: (a) Z=1.7;(b) Z=2.7;(c) Z=2.8 and (d) Z=2.9

In order to determine the effects of the fluid injection on the pressure distribution, the graph of the pressure coefficient distribution is drawn and analysed at different sections for the cases 2 and 3 (Fig. 16 and 17). To compare the two cases, the pressure coefficient distribution of the hydrofoil at transverse section $X = 0.2$ is depicted for both the cases 2 and 3 in Fig. 16(a). Lift coefficient increase in the case 2 comparing to the case 3 is well associated with the increase in pressure difference on the upper and lower surfaces of the hydrofoil , initiated by the injected fluid. Like in the case 1, pressure variation for the case 2 begins farther from the root (Z =1.4 to Z =3) in comparison with the run case without fluid injection ($Z = 1.1$ to Z =3).

The pressure coefficient distribution of the hydrofoil for the cases 2 and 3 at the cross section X = 0.4 is displayed in Fig. 16(b). The pressure variation in the run case without fluid injection occurs in the range from $Z = 1.6$ to $Z = 3$. Clearly, during the injection of the fluid, the difference in pressure on the upper and lower surface of the hydrofoil increases, and consequently, lift increases too. Like in the case 1, it can be seen that in the cross sections adjacent to the leading edge, lift coefficient is greater than that at the trailing edge for the both cases of with and without fluid injection.

As is seen in Fig. 16 (c) and (b), like in the cross section $X = 0.2$ and $X = 0.4$ (see plots (a) and (b)) in comparison with the run case without fluid injection, when fluid injection is conducted, adjacency to the trailing edge yields higher difference in pressure distribution on lower and upper surfaces. Like in the case 1, the interference of the injected fluid with the cross-flow at the tip of the hydrofoil prevents the pressure difference on the upper and lower surfaces from dropping. Flow speed in vicinity of the tip of the hydrofoil increases during the fluid injection (reduction in *w*- value); therefore, *Cp* experiences a sharp reduction which can be revealed by comparing the sections in the run case with fluid injection to the sections in the run case without fluid injection. In all of the sections for the run case with fluid injection, pressure variation at the tip of the hydrofoil is smoother than in the run case without fluid injection.

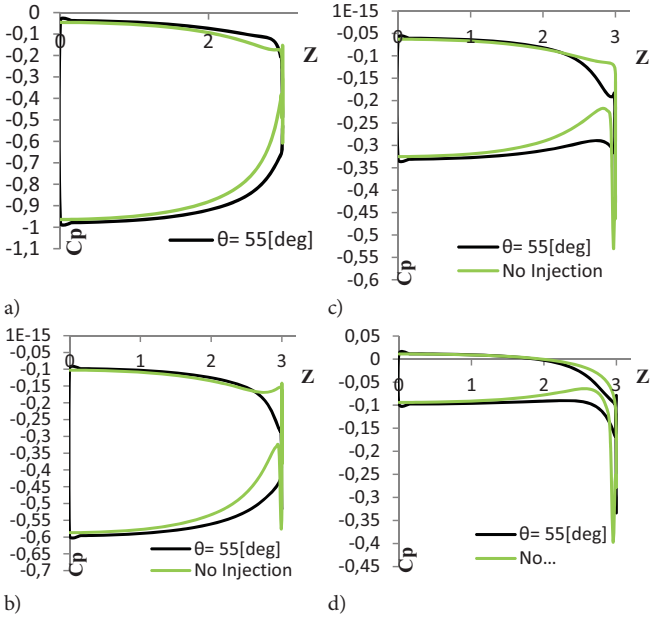

Fig. 16. Effect of the injection angle on distribution of the pressure coefficient Cp in the case 2 : (a) X=0.2; (b) X=0.4; (c) X=0.6 ; (d) X=0.8

In Fig. 17, pressure coefficient distribution is depicted in the different cross sections for the cases 2 and 3. To study the effects of fluid injection on the hydrofoil, Fig. 17(a) has been sketched. Influence of fluid injection on the pressure coefficient distribution is very subtle in cross sections $Z = 1$ in comparison with the run case without fluid injection. Therefore, effects of the fluid injection in the range of $Z = 1$ to $Z = 3$ is quite clear. As displayed in the plots 17 (b), (c), and (d), like in the case 1, when fluid is injected, pressure coefficient difference between the upper and lower surfaces increases in comparison with the run case without fluid injection, and consequently , lift coefficient increases in comparison with the case 3. Like in the case 1, hindrance of vortex formation due to fluid injection is another reason for the increase in the lift force.

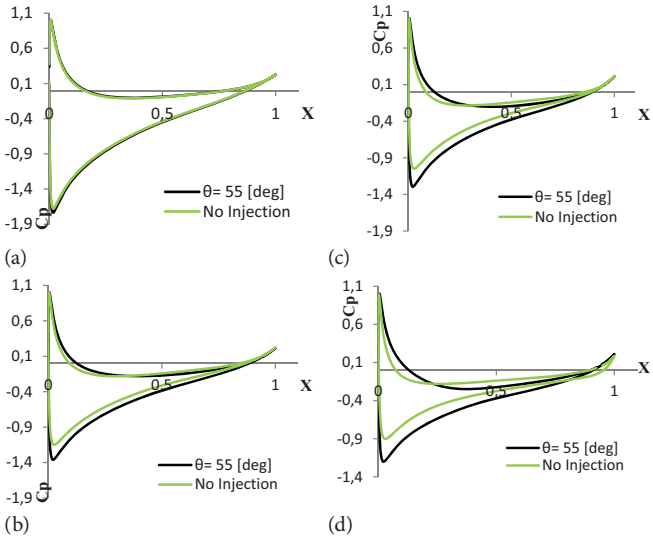

Fig. 17. Effect of the injection angle on distribution of the pressure coefficient Cp in the case 2: (a) Z =1 ; (b) Z =2.7; (c) Z =2.8 ; (d) Z =2.9.

EFFECT OF INJECTION AT TIP VORTICES

In order to acquire a better understanding of the effects of the fluid injection on the tip vortices, pressure contours around the hydrofoil are presented in Fig. 18. In the figure, the three cases : 1) – no injection, 2) – injection with the angle of 55 degrees, and 3) – injection with the angle of -22 degrees) are also presented for Re=1 000 000 and U/V=0.894. The angle of attack is considered to be equal to 6.5 degrees, while the foil body is considered to be rectangular and TR = 1. The chord length is also equal to 1. The pressure contours are presented at the different transverse sections ranging from x/c_R=0 to 0.8. Three injection conditions are considered. In the first condition, no injection is conducted, while the second condition is the case with maximum injection angle of +55 degrees, and the third condition is the case with the minimum injection angle of -22 degrees. Based on the presented contours , it is evident that the injection pushes away the vortices from the tip. In the case with injection angle of +55 degrees, the vortices are directed toward the lower surface of the foil, and in the case with injection angle of -22 degrees, they are directed toward the upper surface. Based on the obtained pressure, it is concluded that during the injection, the area over which negative pressure grows, gets larger; which is why the injection leads to an increase in the lift force.

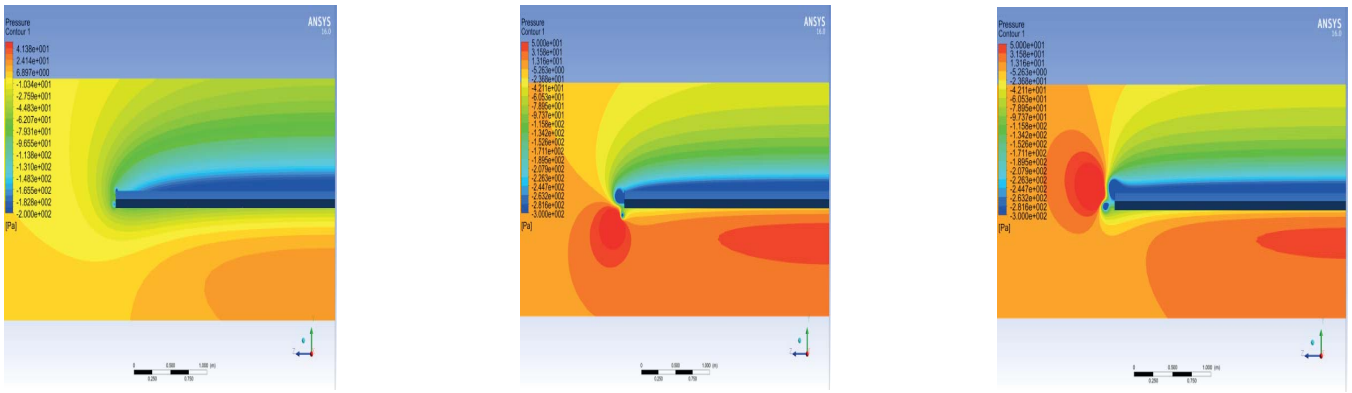

No injection θ=55 θ =-22

X=0.2

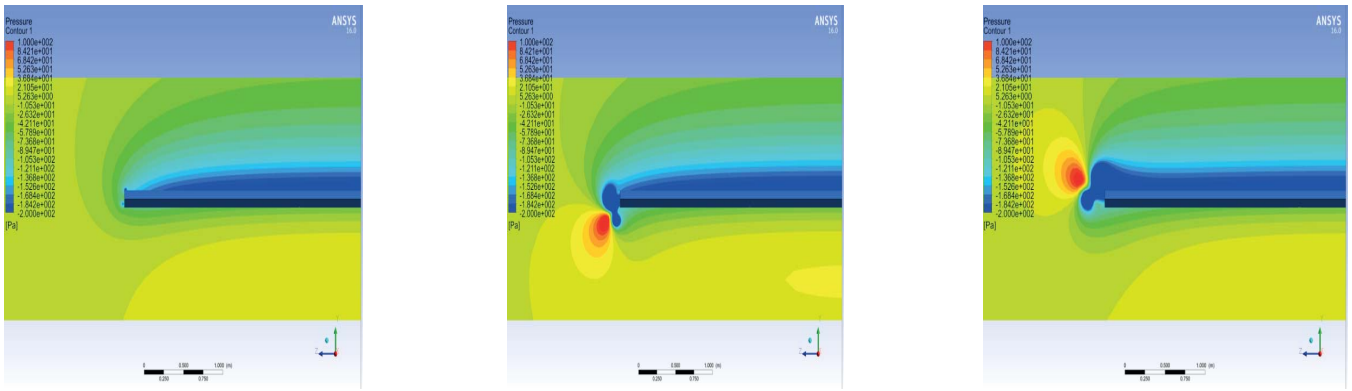

No injection θ=55 θ =-22

X=0.4

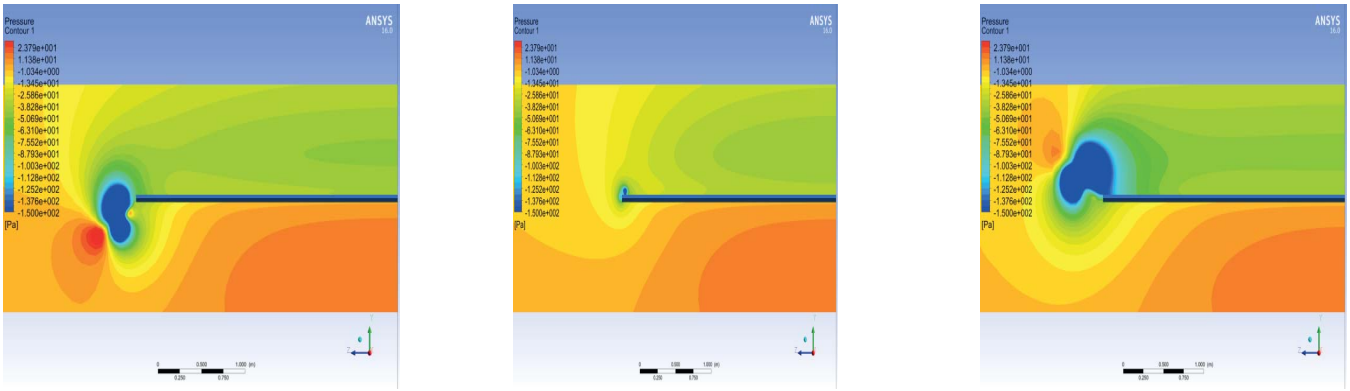

Fig. 18. Pressure contours at different injection condition

CONCLUSIONS

Application of the boundary layer control (BLC) method for controlling flow around bodies and in particular foil sections has recently been receiving wide attention among researchers. In marine engineering, this method is employed to increase the lift- to -drag ratio and efficiency of the hydrofoils. Accordingly, in this paper, effect of the considered method on the hydrodynamic characteristic and tip vortex formation around a hydrofoil is studied. Steady water injection at the tip of the hydrofoil is simulated in different conditions by using ANSYS-CFX commercial software, where the flow is injected in the *yz*-plane.

Results of the simulations indicate that an increase in the injection angle between -20 and 0 degrees at the hydrofoil tip results in an increase in the lift coefficient, while further increase in the range of 0 to 70 degrees reduces the lift coefficient. On the other hand, at the angle of attack equal to 6.5 degrees and for fluid injection angle ranging from -20 to 60 degrees, the drag coefficient shows at first a downward trend and then increases. At the angle of attack of 17 degrees, an increase in the injection angle causes a decrease in the drag coefficient. Based on the definitions of efficiency and efficiency variation percentage, it is observed that fluid injection effects (with regard to the injection location, velocity and angle) at some injection angles are conducive to positive efficiency variation, and at some other angles adversely affects the cross-flow which in turn have an influence on the hydrodynamic performance of the hydrofoil. From the investigations the following results have been obtained:

The most constructive effect on the efficiency occurs for the angle of attack of 6.5 degrees and for the injection angle of 55 degrees. The efficiency variation percentage in this case is 5.21%. For the case with the angle of attack of 6.5 and the injection angle of -20 degree, the negative effect of tip vortices intensifies and the efficiency variation percentage becomes -13.61%. Based on the plots of efficiency variation percentage, it can be observed that BLC method requires a suitable injection angle. Furthermore, the effective system parameters such as fluid injection location, velocity profile, and the fluid injection angle should be properly and carefully selected in order to enhance the performance. It should also be noted that the accuracy of the results also depends on hydrofoil series and geometry.

Moreover, in this paper, the flow pattern during the injection is also studied and it is found that the flow regime is not changed in the neighbourhood of the foil root for all injection angles. Furthermore, effects of injection on the formation of the tip vortices are studied at the maximum and minimum injection angles. At the injection angle of 22 degrees, the vortices are moved upward, and as a result their negative effect on the lift force and pressure is reduced. However, at the maximum injection angle reaching 55 degrees the formed vortices are washed downward.

Finally, it should be noted that the numerical prediction of the drag is less accurate than prediction of the lift; however, the main objective of this paper has been to demonstrate the overall trend of C_d - coefficient corresponding to each angle of injection. In other words, in this paper, the influence of variation of the injection angle on C_d has been investigated. Although, it is probable that the predicted drag is not as accurate as the predicted lift, the overall trend of the drag is accurate enough to show the effect of injection or angle of injection on the performance of the hydrofoil.

Future studies related to this work include investigation of the effects of time-harmonic-injection by which some other effects may be observed. Furthermore, coupling of the present simulation with an optimization algorithm for finding an optimized injection condition for the rudder of an underwater vehicle is another important future task.

ACKNOWLEGMENT

This research received no specific grant from any funding agency in the public, commercial, or non-profit sectors, hence there is no conflict of interest.

REFERENCES

1. Kroo, I. : *Non-planar wings concepts for increases aircraft efficiency.* VKI lecture series on Innovative Configurations and Advanced Concepts for Future Civil Aircraft, 2005.

2. Park, K., Lee J. *Influence of endplate on aerodynamic characteristics of low-aspect ratio wing in ground effect*. J. Mech. Sci. Tech., 22, 2578-2589, 2008.

3. Kaplan S.M., Altman A. : *Wake Vortices Measurements for Low Aspect Ratio Wings at Low Reynolds Number*. J. Aircraft. 44, 1631-1639, 2007.

4. Mansour, N.N. : *Numerical Simulation of the Tip Vortex of a Low Aspect Ratio Wing at Transonic Speed*. AIAA, 23, 1143-1149, 1985.

5. McAlister, K.W., Takashi T.K. : *NACA 0015 Wing Pressure and Trailing Vortex Measurements*. ACSOM Technical Report 91-A-003, California, 1991.

6. Mariani, J., Zilliac G., Chow J., Bradshaw P. : *Numerical/ Experimental Study of a Wingtip Vortex in the Near Field*. AIAA, 33. 1561-1568, 1995.

7. Englar, R.J. : *Circulation control for high lift and drag generation on STOL aircraft*. . J. Aircraft, 12, 457-463, 1975.

8. Englar, R.J. Trabouh, L.A., Hemmersly R. : *STOL potential of the circulation control wing for high-performance aircraft*. J. Aircraft, 25, 236-243, 1978.

9. Wood, N. Nielsen J.: *Circulation control airfoils-past, present, future*. AIAA. 85-0204, 23rd Aerospace Sciences Meeting, Reno, Nevada, 1985.

10. Wood, N. and Robert, L. : *Control of vortical lift on Delta wings by tangential leading-edge blowing*. J. Aircraft, 25, 236-243, 1988.

11. Wood, N., Robert, L. and Celik Z. : *Control of asymmetric vertical flows over delta wings at high angle of attack*. J. Aircraft. 27, 429-435, 1990.

12. Modi, V. Fernando, M. Yokomizo, T. : *Drag reduction of bluff bodies through moving surface boundary layer control*. AIAA Paper No. 1990-298, 28th Aerospace Sciences Meeting, Reno, Nevada, 1990.

13. Johari, H. and MaManus, K. *: Visualization of pulsed vortex generator jets for active control of boundary layer separation*. AIAA Paper 1997-2021, 28th Fluid Dynamic Conference, Snowmass Village, Colorado, 1997.

14. McManus, K. Magill, J. : *Airfoil performance enhancement using pulsed jet separation control*. AIAA Paper 1997-1971, 4th Shear Flow Control Conference, Snowmass Village, Colorado, June 29-July 2, 1997.

15. Zha G, Paxton C. : *A novel airfoil circulation augment flow control method using co-flow jet*. AIAA Paper 2004-2208, 2nd AIAA Flow Control Conference, Portland, Oregon, 2004.

16. Zha, G., Carrol, B., Paxton, C., Conely C., Wells, A. : *High Performance Airfoil Using Co-Flow Jet Flow Control*. AIAA Paper 2005-1260, 43rd Aerospace Sciences Meeting, Reno, Nevada, 2005.

17. Gilarranz, J.L., Traun. L.W., Radiniotis. O.K. : *A new class of synthetic jet actuators-part 1: design, fabrication and bench top characterization*. J. Fluids Eng. 127, 367-376, 2005.

18. Gilarranz, J.L., Traun. L.W., Radiniotis. O.K. : *A new class of synthetic jet actuators-part 2: Application to flow separation control*. J. Fluids Eng. 127, 377-387, 2005.

19. You, D., Moin, P. : *Active control of flow separation over an airfoil using synthetic jets*. J. Fluids Struct. 24, 1349-1357, 2008.

20. Agrawal, G., Rediniotis, O.K., Taub, L.W. : *An experimental investigation on the effects of pulsed air blowing separation control on NACA 0015*. 46th AIAA Aerospace Sciences Meeting and Exhibit, Reno, NV. AIAA Journal, 0, 1-12, 2005. ?

21. Mack, S. Berhm, C., Heine B., Kurz, A., Fasel, H. F. : *Experimental investigation of separation and separation control on a laminar airfoil*. 4th AIAA Flow Control Conference. Seattle, WA, 2008.

22. Gompertz, K. Bones, J.P. : *Combined unsteady wakes and active flow control on a low-pressure turbine airfoil*. J. Prop. Power, 5, 990-1000, 2011.

23. Packard, N. O. Thakejr, M. P., Bonilla, C. H., Gompertz, K, Bones, J. : *Active control of flow separation on a laminar aircraft*. AIAA Journal. 51, (5), 1032-1041, 2013.

24. Gardner, A.D., Ritchter, K., Neuhaus, D. Experimental investigation of high-pressure pulsed blowing for dynamic stall control, CAES Aeronautical J, 5, 185-198, 2014.

25. Zhang, W., Samataney, R. A. : *Direct numerical simulation investigation of the synthetic jet frequency effects on separation control of low-Re flow past an airfoil*. Physics of Fluids, 27, 055101, 2015.

26. Mang, X., Yan, X., Hu, H., Liu, F., Luo, S. : *Plasma laminar-separation-bubble control over airfoil at low Reynolds numbers*. 46th AIAA Plasmadynamics and Lasers Conference, 2015.

27. Hipp, K.D., Walker, M., Benton, S.I., Bones, J. : *Control of leading-edge airfoil stall using pulsed jets*. 54th AIAA Aerospace Sciences Meeting, 2016.

28. Bernardini, C., Beneton S. I., Hipp, K. D., Bons, J. P. : *Large low-frequency oscillations initiated by flow control on a poststall airfoil*, ? 2016.

29. Ghadimi, P., Kermani, S., Feizi Chakab, M.A. : *Numerical hydro-acoustic analysis of NACA foils in marine applications and comparison of their acoustic behavior*. ISRN Mech. Eng., 2013, 1-12, 2013.

30. Kelterer ME, Pecnik R, Sanz W. : *Computation of Laminar-Turbulent Transition in Turbumachinery Using the Correlation Based γ-Reθ Transition Model*. ASME Proceedings, Turbomachinery, 7, 613-622.

31. Counsil J.N., Boulama K.G. 2013? : *Low-Reynolds-Number Aerodynamic Performances of the NACA 0012 and Selig–Donovan 7003 Airfoils*. J Aircraft, 50(1), 204-216. 2010

32. Khayatzadeh P. , Nadarajah S. : *Aerodynamic Shape Optimization via Discrete Viscous Adjoint Equations for the k-wSST Turbulence and γ-Re0 Transition Models*. In: 49th AIAA Aerospace Sciences Meeting including the New Horizons Forum and Aerospace Exposition, Orlando, Florida, US. 2011.

33. Menter, F.R. : *Two equation eddy-viscosity turbulence models for aerodynamics for engineering applications*. AIAA J. 32(8). 1598-1605. 1994.

34. Ansys CFX User's Manual 2013.

34. McCormick, D. : *Boundary Layer Separation Control With Directed Synthetic Jets*. AIAA Paper No. 2000-0519, 2011.

CONTACT WITH THE AUTHORS

Parviz Ghadimi
e-mail: pghadimi@aut.ac.ir
Amirkabir University of Technology
424 Hafez Ave., 3314 Tehran
Islamic Republic of Iran

Araz Tanha
e-mail: araz.tanha@aut.ac.ir
Amirkabir University of Technology
424 Hafez Ave., 3314 Tehran, Iran
Islamic Republic of Iran

Navid Nemati Kourabbasloo
e-mail: Nemati_n@mech.edu
Sharif University of Technology
Azadi Ave., 9090 Tehran
Islamic Republic of Iran

Sasan Tavakoli
e-mail: sasan_tavakoli@aut.ac.ir
Amirkabir University of Technology
424 Hafez Ave., 03314 Tehran
Islamic Republic of Iran